# Supplementary material:
# Ultra-broadband terahertz coherent detection via a silicon nitride-based deep sub-wavelength metallic slit

A. Tomasino,[1,2] R. Piccoli,[1,a] Y. Jestin,[1] S. Delprat,[1] M. Chaker,[1] M. Peccianti,[3] M. Clerici,[4] A. Busacca,[2] L. Razzari,[1] and R. Morandotti[1,5,6,b]

[1]*INRS-EMT, 1650 Boulevard Lionel-Boulet, Varennes, Québec, J3X 1S2, Canada*

[2]*DEIM, University of Palermo, Viale delle Science Ed. 9, Palermo, 90128, Italy*

[3]*Department of Physics and Astronomy, University of Sussex, Falmer, Brighton, BN1 9RH, United Kingdom*

[4]*School of Engineering, University of Glasgow, Glasgow, G12 8LT, United Kingdom*

[5]*ITMO University, Mechanics and Optics, St. Petersburg 199034, Russia*

[6]*Institute of Fundamental and Frontier Sciences, University of Electronic Science and Technology of China, Chengdu 610054, Sichuan, China.*

## METHODS

In this Section, we present the detailed description of the simulations carried out to accurately estimate the THz field enhancement (FE) induced by the SiN-embedded slit. We start by modeling the emission pattern of the ultra-broadband two-color THz plasma source. Then, by considering simple geometrical principles, which include the analytical description of the frequency dependent collimation and subsequent focusing of the THz beam via two parabolic mirrors, we define the initial condition of the profiles associated to different beam spectral components. We then employ those values in the simulations.

## THz BEAM PROPAGATION MODELING AND FIELD ENHANCEMENT SIMULATION

To estimate the THz FE in our SSBCD device, we properly refine the methodology previously employed for the low and narrow frequency range of 0.1-1 THz. In our case, the frequency-dependent focusing of the THz beam onto the slit cannot be neglected due to its ultra-broadband nature. Let us consider a fixed diameter for all the collimated input spectral beam components. At a first approximation, higher frequencies are tightly focused to smaller spots (resulting in higher peak values on the slit center) with respect to those at lower frequencies. Conversely, by considering the same peak value, the larger spots associated to lower frequencies result in a higher field enhancement. These concurrent effects determine the ultimate frequency response of the slit. In addition, the presence of a dielectric material surrounding the slit affects the total FE. Let us consider the experimental set-up sketched in Fig. S1. The infrared (IR) 140-fs-long pump pulse and its second harmonic (SH, generated in a 100-μm-thick BBO crystal) are focused together through a 4-inch off-axis mirror, thus generating a plasma channel with length equal to $L$ = 7 mm and $1/e^2$ radius of $r$ = 50 μm, measured by acquiring the fluorescence of the filament via a CCD camera. We assumed that the plasma emits THz pulses with a frequency content approximately spanning the range of 0.1-10 THz. For our purpose, it is therefore convenient to regard the THz wave as the superposition of several beam components at different frequencies. Each component diffracts with an angular distributed interference pattern, whose frequency-dependent maxima are formed at an angle $\theta$ estimated by means of the formula[1]:

$$\theta(\omega) \approx \sqrt{\frac{\lambda}{L}} = \sqrt{\frac{2\pi c}{\omega L}}. \tag{S1}$$

[a] Electronic email: riccardo.piccoli@inrs.emt.ca

[b] Electronic email: morandotti@inrs.emt.ca

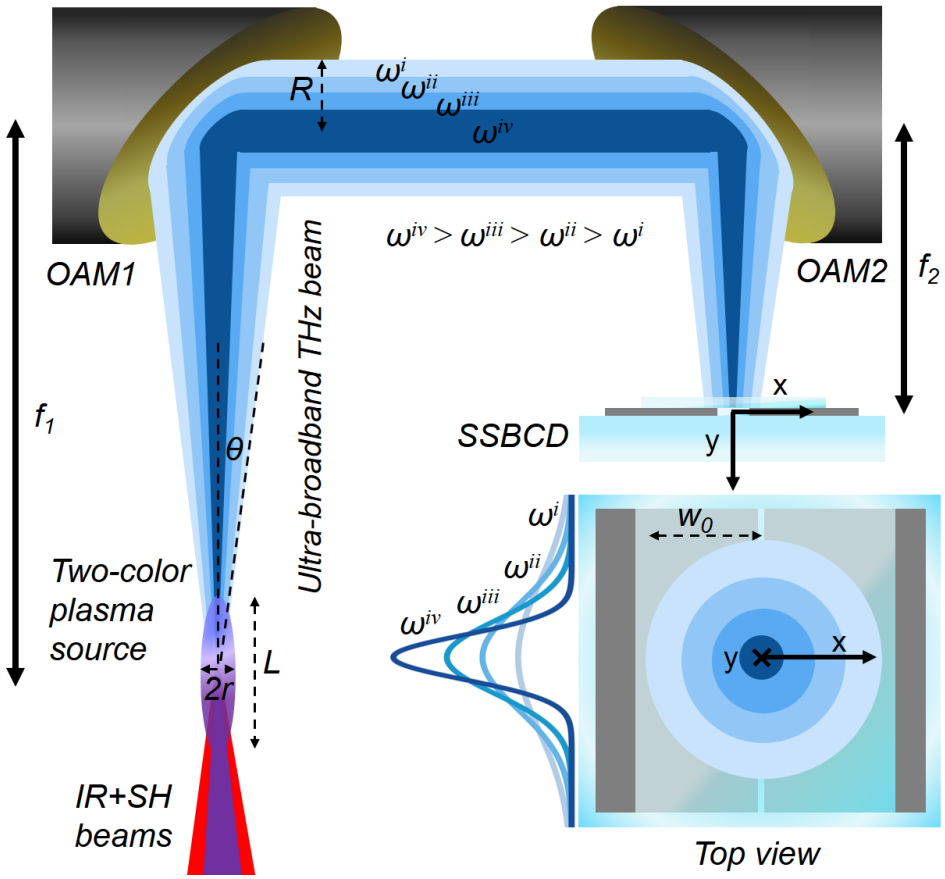


FIG. S1: Geometry of the ultra-broadband THz set-up considered for the modeling of the THz field enhancement. An infrared pulsed beam (IR) and its second harmonic (SH) are focused together in air to generate a two-color plasma channel with length $L$ and radius $r$, acting as a source emitting THz pulses with a frequency content approximatively spanning the 0.1-10 THz range. The THz beam is regarded as the superposition of several frequency components (different shades of blue) featured by distinct emission cones, whose aperture angle is indicated with $\theta$. The first mirror OAM1 with focal length $f_1$ collimates the beam (to a radius $1/e^2$ R), whereas a second mirror OAM2 with focal length $f_2$ focuses the beam onto the SSBCD device. The plane of the sub-λ slit overlaps the focal plane of OAM1, where each frequency component of the THz beam features a waist size $w_0$, as indicated in the bottom right inset. Here, we show a top view of the device and an example of the different field profiles associated to each frequency component (darker shades of blue correspond to higher frequencies).

Here, $\lambda$ is the THz wavelength in vacuum, $\omega$ the THz angular frequency and $c$ the speed of light. Equation S1 states that the higher the frequency, the smaller the emission angle, as sketched in Fig. S1, where darker shades of blue correspond to higher frequencies. The first 90° off-axis mirror OAM1 collects and collimates the THz beam, whose frequency-dependent radius $R$ is evaluated as:

$$R(\omega) \approx \min\left[\frac{D}{2}, f_1 \tan\left(\theta(\omega)\right) + r\right], \tag{S2}$$

where $D$ and $f_1$ are the diameter and the effective focal length of the mirror, respectively. For the sake of completeness, we considered the possibility that some frequency components (< 0.5 THz) could result in beam diameters wider than the clear aperture of the mirror. The collimated THz beam is then focused by a second 90° off-axis mirror (OAM2) - with effective focal length $f_2$- into a spot size, whose frequency-dependent waist $w_0$ can be evaluated as[2]:

$$w_0(\omega) \approx \frac{\lambda f_2}{\pi R(\omega)} = \frac{2cf_2}{\omega R(\omega)}. \tag{S3}$$

Equation S3 represents the case of a beam focused in air. For the case of the SSBCD device placed at the detection position, we assume that the plane of the slit overlaps the focal plane of the mirror.

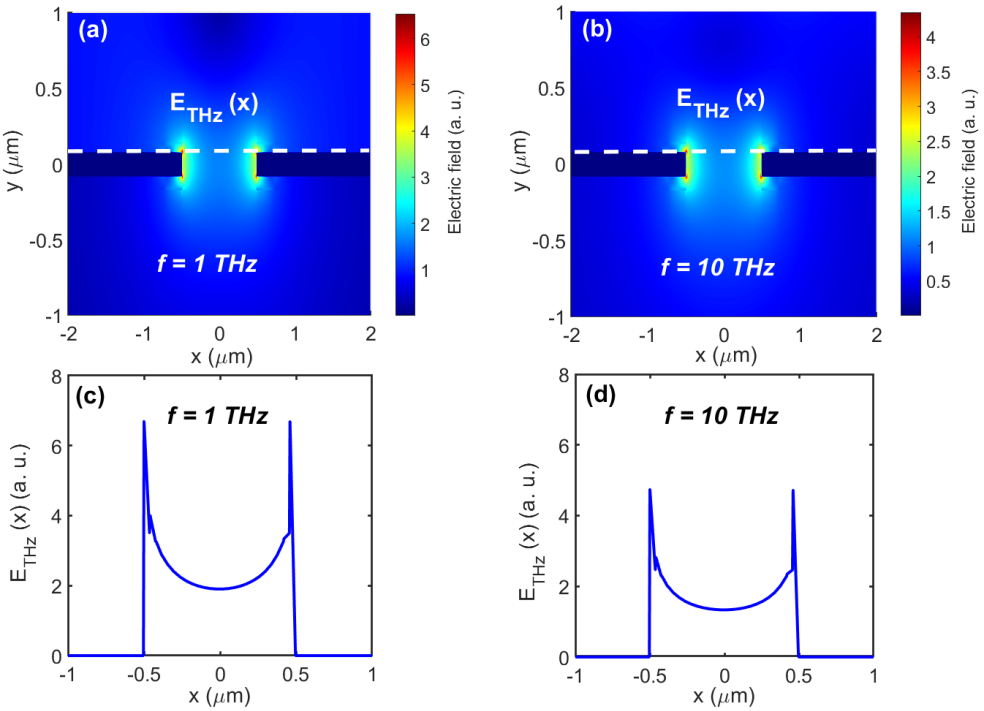


FIG. S2: 2D distribution of the THz electric field in the slit for the frequency component of 1 THz (a) and 10 THz (b). The corresponding profiles of the THz electric fields at 1 THz and 10 THz, evaluated along the white dashed lines, are plotted in (c) and (d), respectively.

This means that the THz beam has to travel inside the 1-μm-thick SiN cover layer while is being focused, before reaching the metal contacts. However, due to the subwavelength thickness of the cover layer, we neglected the extremely small deviation, which the THz wave experiences due to the refraction of the beam at the air/SiN interface (evaluated as only few hundreds of nanometers at 10 THz, diminishing as the frequency decreases). The knowledge of $w_0$ serves to evaluate the initial condition that needs to be imposed to each beam component profile in order to properly model the focusing onto the slit. In particular, for our simulations, we considered a 2D *x*-*y* reference system with origin on the center of the slit, where *x* is the transversal axis and *y* is the propagation direction (see Fig. S1). In this way, by noting that the system made up by two off-axis mirrors is a telescope with magnification $f_2/f_1 < 1$, the transversal profile of each THz electric field component impinging on the device assumes the form:

$$E_{THz}(x,\omega) \propto \frac{r}{w_0(\omega)} \exp\left[-\left(\frac{x}{w_0(\omega)}\right)^2\right] \tag{S4}$$

Equation S4 represents the input condition used to simulate the THz electric field propagating through the device. In order to account for the presence of the dielectric material surrounding the slit, we experimentally evaluated the refractive index of silicon nitride in the THz spectral range. This was achieved by means of a differential time-domain spectroscopy algorithm[3] applied to a set of measurements carried out on a 10-μm-thick film of PECVD-grown SiN, deposited on a 500-μm-thick quartz substrate. We estimated a refractive index of 2.45, with losses in the order of few $cm^{-1}$, which we neglected because of the ultra-thin thickness of the cover layer. The metal pads of the slit were modeled as a 2×2 $mm^2$ stack of metal sheets made up by a 100-nm-thick aluminum layer sandwiched between two 30-nm-thick layers of chromium. In our calculations, we further accounted for the real spectral response of the two metals in the whole THz range, by evaluating their complex frequency-dependent dielectric parameter via a Drude model[4,5]. We performed two sets of simulations in the range 0.25-10 THz (with a step of 0.25 THz between 0.25 and 1 THz and 0.5 THz between 1 and 10 THz), evaluating the THz electric field at its focus, once for the case of a unique layer of SiN (background field) and then when the metallic slit is also present. In Fig. 2(a) and (b), we report the 2D field distribution calculated at 1 and 10 THz, respectively, for the second case. In particular, Fig. 2(c) and (d) show the transversal profiles of the THz electric field evaluated along the white dashed lines (5 nm above the metal pad edge)

plotted in (a) and (b), respectively. A significant confinement of the electric field within the slit (centered at the origin of the *x*-axis) can be noticed, which is stronger close to the edges of the metal pads. Therefore, we calculated the mean value of the THz electric field by integrating its transverse profiles (like those in Fig. 2(c) and (d)) over the *x* coordinate for a region as wide as the slit extension, either with or without (background field) the slit. These values are plotted in Fig. S3 for (a) $E_{THz}^{slit}$ and (b) $E_{THz}^{back}$. Finally, the FE is evaluated for each frequency component as the ratio between the two average fields:

$$FE(\omega) = \frac{\left\langle E_{THz}^{slit}(\omega) \right\rangle}{\left\langle E_{THz}^{back}(\omega) \right\rangle}. \tag{S5}$$

The FE calculated according to Eq. S5 as a function of the frequency is shown in Fig. 2(b) of the main text. For simplicity, here we report its trend in Fig. S4 (blue dotted line), together with a best fit, demonstrating a numerical $\sim 1/f^{0.63}$ dependence upon the frequency, which slightly differs from the $1/f$-trend found in literature under the hypothesis of an unlimited slit uniformly illuminated by a plane wave[6]. The main reasons behind such a difference have to be ascribed to the finite slit size and the different focal spot associated to the focused THz beam. Moreover, in our work the real dimensions of the device (gap size of 1 μm and metal pad thickness of 160 nm) actually define a completely different geometrical regime with respect to Ref. 6 (where, instead, the gap size was much smaller than the metal pad thickness).

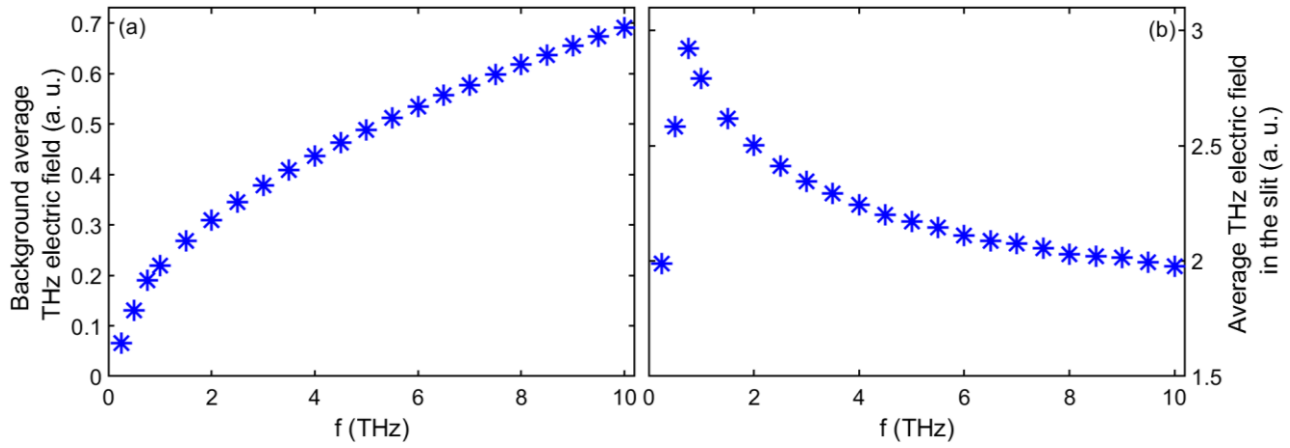


FIG. S3: (a) Average THz electric field $E_{THz}^{slit}$ as a function of the frequency calculated for the background field. (b) Average THz electric field $E_{THz}^{back}$ as a function of the frequency calculated for the slit.

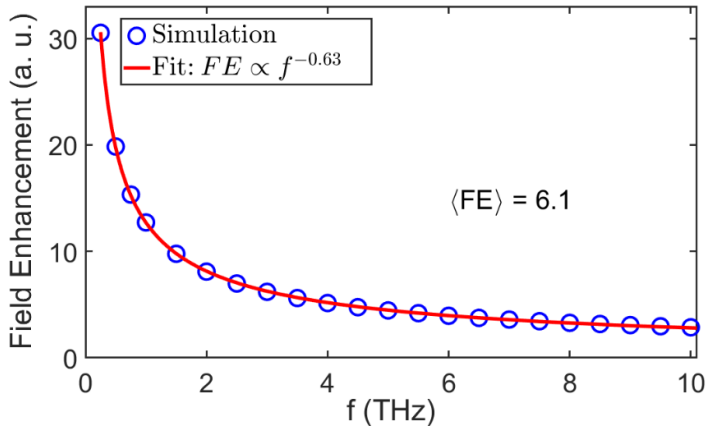


FIG. S4: Calculated FE as a function of the frequency (blue dotted line). The fit (red solid line) reveal a numerical $1/f^{0.63}$ dependence upon the frequency.

**REFERENCES**

[1] C.D. Amico, A. Houard, S. Akturk, Y. Liu, J. Le Bloas, M. Franco, B. Prade, A. Couairon, V.T. Tikhonchuk, and A. Mysyrowicz, New J. Phys. **10**, 013015 (2008).

[2] A. Tomasino, A. Parisi, S. Stivala, P. Livreri, A.C. Cino, A.C. Busacca, M. Peccianti, and R. Morandotti, Sci. Rep. **3**, 3116 (2013).

[3] Z. Jiang, M. Li, and X.-C. Zhang, Appl. Phys. Lett. **76**, 3221 (2000).

[4] M.A. Ordal, L.L. Long, R.J. Bell, S.E. Bell, R.R. Bell, R.W. Alexander, and C.A. Ward, Appl. Opt. **22**, 1099 (1983).

[5] R. Lovrinčić and A. Pucci, Phys. Rev. B - **80**, 205404 (2009).

[6] J.-H. Kang, D.-S. Kim, and M. Seo, Nanophotonics **7**, 763 (2018).